Supporting information

Sulfone-functionalized Stereoisomeric [3]Radialene Displays Guest-induced Modulation of Porous Frameworks and Critical Crystallization-induced Near-infrared Emission

Gaoqiang Xu[1,2], Ying Zhao[1], Sheng Xie[1, 3*], Zhibiao Zhou[1,4], Ziyu Luo[5], Haohao Liu[1], Yang Zhang[1], Zijie Qiu[2], Anlian Pan[5*], Zebing Zeng[1*], Ben Zhong Tang[2*]

[1]State Key Laboratory of Chemo and Biosensing, College of Chemistry and Chemical Engineering, Hunan University, Changsha 410082, China;
[2]Guangdong Basic Research Center of Excellence for Aggregate Science, School of Science and Engineering, Shenzhen Institute of Aggregate Science and Technology, The Chinese University of Hong Kong, Shenzhen (CUHK-Shenzhen), Guangdong 518172, China;
[3]Shenzhen Research Institute, Hunan University, Shenzhen 518000, China ;
[4]TCM and Ethnomedicine Innovation and Development International Laboratory, Innovative Materia Medica Research Institute, School of Pharmacy, Hunan University of Chinese Medicine, Changsha, China;
[5]Hunan Institute of Optoelectronic Integration, College of Materials Science and Engineering, Hunan University, Changsha 410082, China.

Table of contents

General methods

All Solvents were purified and dried by standard methods prior to use. Other commercially available reagents were used without further purification unless otherwise noted. Reactions were monitored by thin layer chromatography (TLC) using silica gel GF254 plates with UV light to visualize the course of reaction and column chromatography was generally performed on silica gel (200-300 mesh). ^{1}H and ^{13}C NMR spectra were recorded on a Bruker 400 MHz spectrometer. The following abbreviations were used to explain the multiplicities: s = singlet, d = doublet, t = triplet, m = multiplet. Absorption spectra were recorded on a SHIMADZU UV-3600 plus. Photoluminescence spectra were recorded on Edinburgh FLS1000 spectrometer. The fluorescent quantum yields in solid state were measured using an integrating sphere by an Edinburgh FLS1000. High-resolution mass spectra (HRMS) were recorded on a Finnigan MAT TSQ 7000 spectrometer system operating in a MALDI-TOF mode. Photoluminescence decay traces were collected by employing time-correlated single-photon-counting (TCSPC) technique using an Edinburgh FLS1000 through a motorized monochromator. Solvent-accessible void spaces was estimated by Platon.[S1] TGA test was conducted on STA8000, the sample is first held at 40 °C in a nitrogen atmosphere for 1 hour, then cooled to room temperature. Next, it is heated to 800 °C at a rate of 5 °C/min while data is collected. BET test was conducted on AUTOSORB IQ, prior to data collection, the samples were degassed at 100 °C for 8 h. The aggregation effect was considered by using ONIOM method with QM and MM layers in Gaussian 16 program.[S2] The UFF force field was used with the restrained electrostatic potential (RESP) partial charges for the MM treatment. And the computation model for solid phase was built by digging a cluster from the X-ray crystal. All calculations of geometry optimizations and vibrational frequency for the ground state (S_0) and the first excited state (S_1) of gas phase were respectively studied by using the restricted density functional theory (DFT) and TD-DFT by B3lyp/6-31g(d,p) basis sets. A full Natural Bond Orbital (NBO) analysis have been done by Gaussian16 program to give a clear view on electronic population, and the analysis data of molecular orbital composition were generated by Multiwfn package.[S3-S4] Based on the trimer structure within the crystal, we analyzed the electron density changes before and after molecular packing, along with the intermolecular interactions. The wave function of the trimer was computed at the B3LYP-D3/def2-SVP level using the ORCA 5.0 quantum chemistry package.[S5-S8] Theoretical analyses, including the study of weak intermolecular interactions via the Independent Gradient Model based on Hirshfeld partition (IGMH), as well as calculations of electron density differences, were performed using the Multiwfn 3.8(dev) program.[S9] All corresponding isosurface maps—such as electron density differences and non-covalent interactions—were generated with Multiwfn

3.8(dev) and rendered using VMD 1.9.3. [S10]

Synthetic procedure

Compound thioxanthene was synthesized according to reported literature [S11].

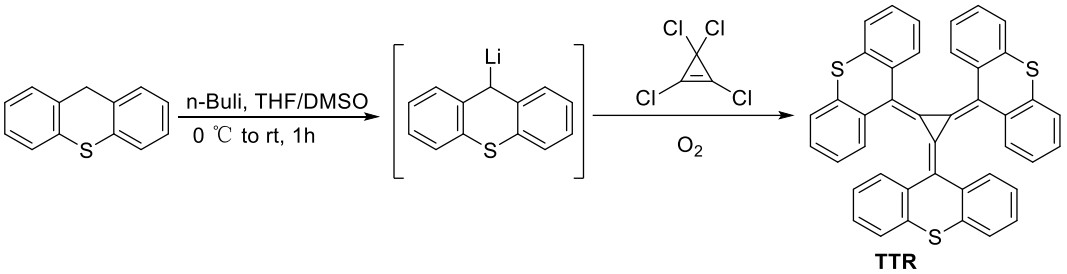

To a flame-dried 100 mL Schlenk tube, 10 mL dry THF and 10 mL dry DMSO was added under argon atmosphere. The solution was cooled to 0 ºC and *n*-BuLi solution (1.6 M in *n*-hexane, 0. 9 mL, 1. 51 mmol) was slowly added. The mixture was stirred for 10 minutes at 0 ºC. Afterwards, a soultion of compound thioxanthene (300 mg, 1.51 mmol) in dry THF was added solwly and the mixture was stired for 1h at 0 ºC. Then, **TCCP** (44.8 mg, 0.25 mmol) dissolved in 2.5 mL dry THF was added dropwise via syringe. The mixture was stirred at 0 ºC for 30 min, then at room temperature for another 30 min, and aganin cooled to 0 ºC. Oxygen was bubled into the reaction for 30 min at 0 ºC and another 30 min at room temperature. Then, water (50 mL) was added into the reaction and the mixture was extracted with DCM (3 × 50 mL). The organic phase was dried over Na_2SO_4. The solvent was removed under vacuum and the residue was further purified by chromatography using silica-gel (Petroleum ether/CH_2Cl_2 = 10:1, R_f = 0.5) to afford **TTR** (42.5 mg, 27%). ^{1}H NMR (400 MHz, $CDCl_3$) δ 7.38 (d, *J* = 7.7 Hz, 6H), 7.09 (t, *J* = 7.6 Hz, 6H), 6.86 (d, *J* = 7.8 Hz, 6H), 6.47 (t, *J* = 7.6 Hz, 6H). ^{13}C NMR (100 MHz, $CDCl_3$) δ 134.8, 132.6, 130.3, 127.0, 125.1, 124.8, 119.8, 116.5. HRMS (MALDI-TOF, m/z) calcd for $C_{42}H_{24}S_3^+$ [M] $^+$ = 624. 1040; found 624.1042 (error = +0.32 ppm).

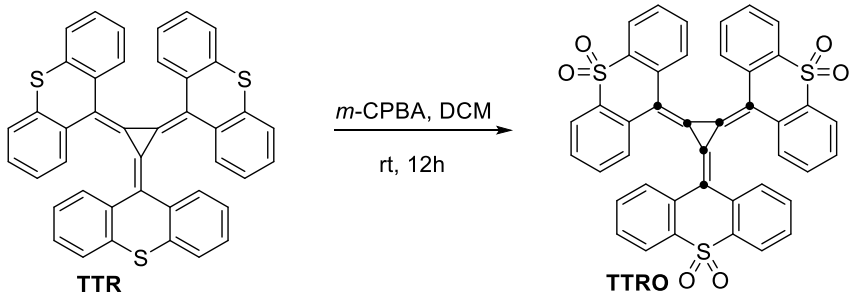

Compound **TTR** (90 mg, 0.14 mmol) and *m*-CPBA (149.3 mg, 0.87 mmol) were added under an argon atmosphere. Then, 30 mL dry DCM was added and the reaction was stired 12h at room tenperature. Then, the reaction mixture was washed with saturated sodium bicarbonate solution (3 × 50 mL). The organic phase was dried over Na_2SO_4. The solvent was removed under vacuum and the residue was further purified

chromatography using silica-gel (Petroleum ether/EA = 3:1, R_f = 0.4) to afford **TTRO** (95.3 mg, 92%). ^{1}H NMR (400 MHz, $CDCl_3$) δ 8.17 (d, *J* = 7.3 Hz, 6H), 7.46 (t, *J* = 7.9 Hz, 6H), 7.09 (d, *J* = 7.7 Hz, 6H), 6.99 (t, *J* = 6.8 Hz, 6H). ^{13}C NMR (100 MHz, $CDCl_3$) δ 136.4, 135.8, 130.9, 130.0, 129.1, 123.5, 121.4, 116.5. HRMS (MALDI-TOF, m/z) calcd for $C_{42}H_{24}NaO_6S_3^+$ [M+Na^+] = 743.0627; found 743.0625 (error = −0.27 ppm).

Prepareation for the single crystal sample

Hex@TTRO: At room temperature, n-hexane was allowed to slowly diffuse into a chloroform solution of **TTRO** (20 mg/mL), and the corresponding crystalline samples were obtained after approximately two days.
THF@TTRO: At room temperature, cyclohexane was allowed to slowly diffuse into a THF solution of **TTRO** (20 mg/mL), and the corresponding crystalline samples were obtained after approximately seven days.
Non@TTRO and **DMF/MeOH@TTRO**: 15 mL of DMF and 3 mL of methanol were added to a sample vial and mixed thoroughly, followed by the addition of 30 mg of **TTRO**. The mixture was sonicated until complete dissolution was achieved and then left to stand at room temperature for approximately one month, affording the corresponding two types of single-crystal samples.

^{1}H and ^{13}C NMR spectra

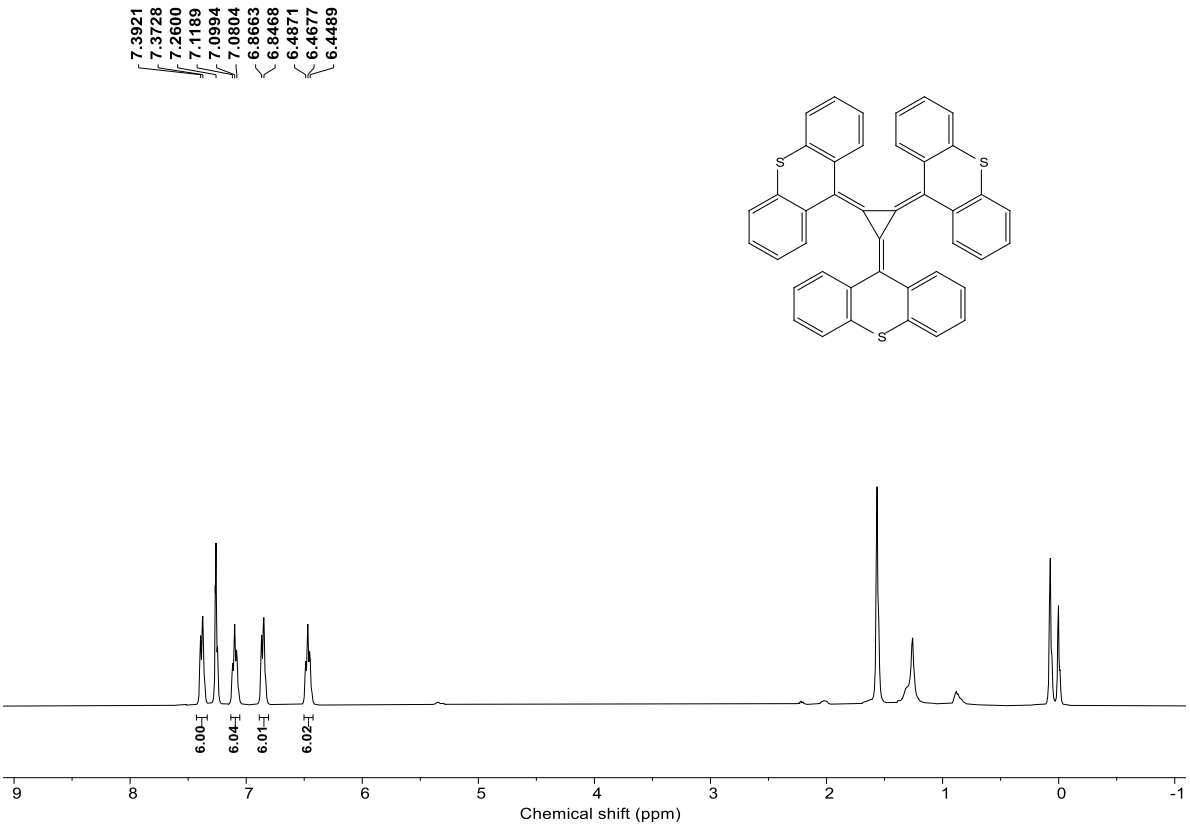

Figure S1. ^{1}H NMR spectrum (400 MHz) of compound **TTR** in $CDCl_3$ at 298 K.

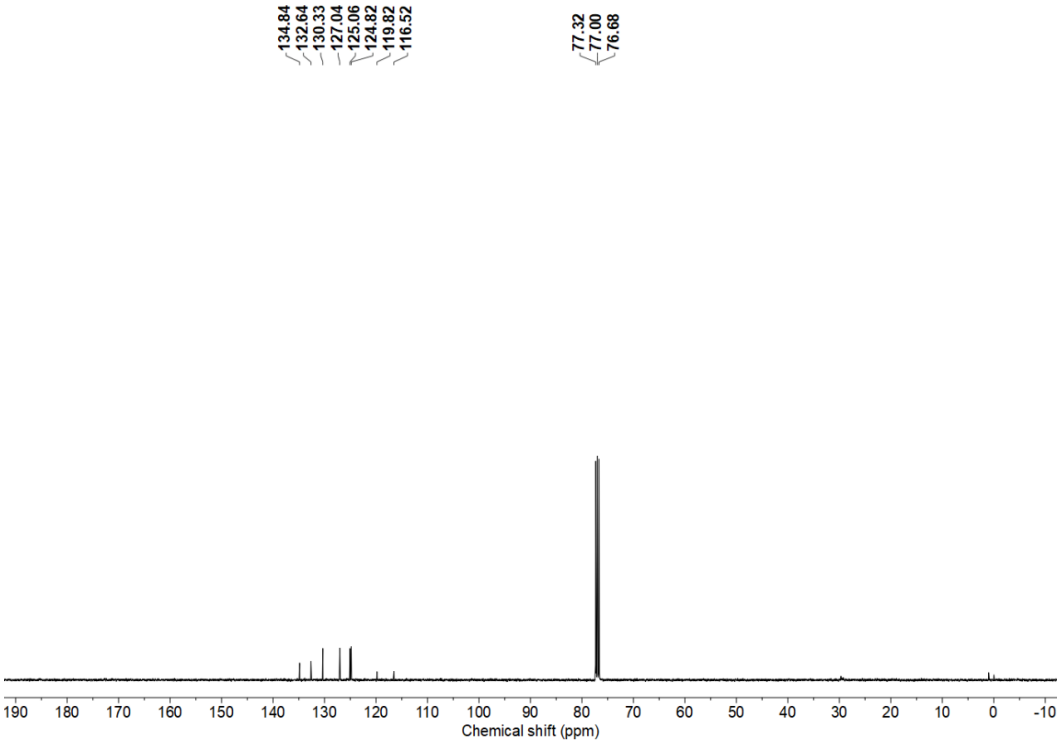

Figure S2. ^{13}C NMR spectrum (100 MHz) of compound **TTR** in $CDCl_3$ at 298 K.

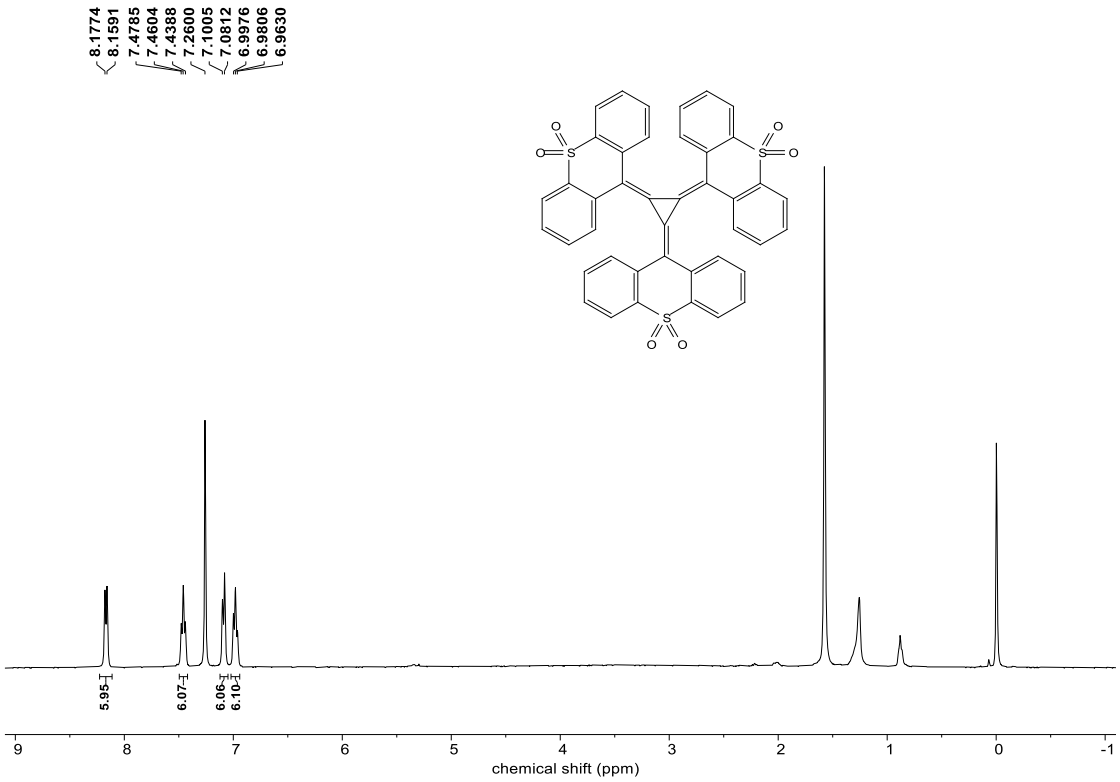

Figure S3. ^{1}H NMR spectrum (400 MHz) of compound **TTRO** in $CDCl_3$ at 298 K.

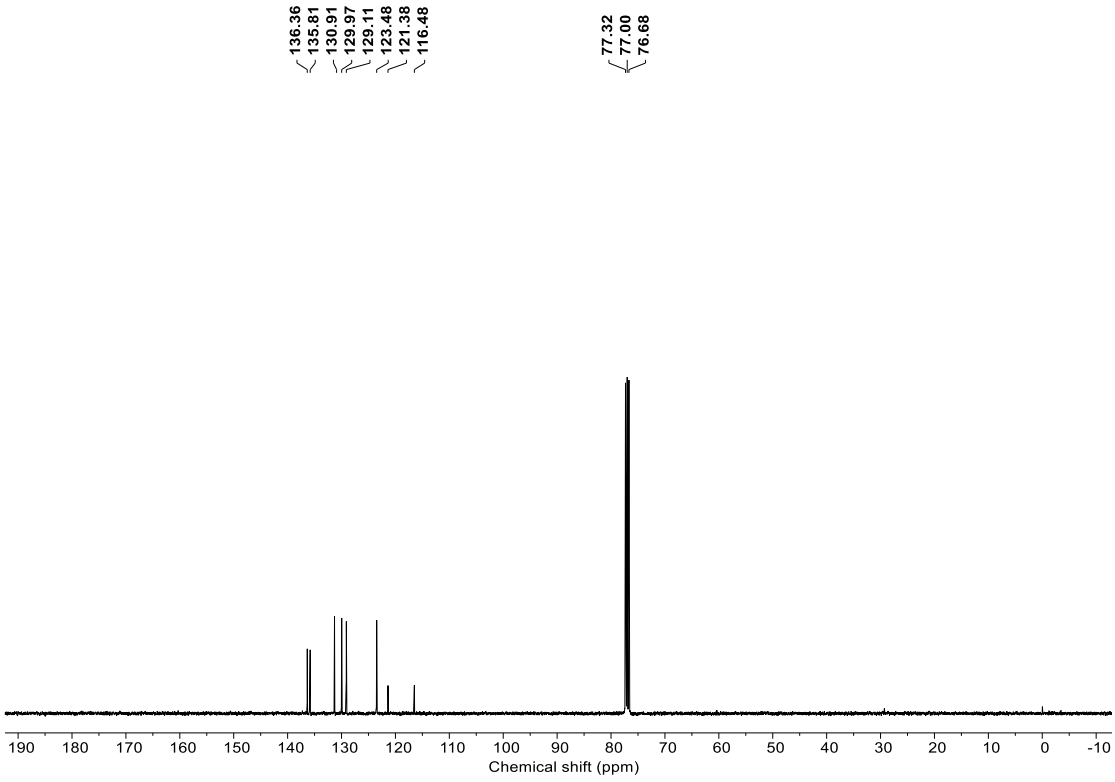

Figure S4. ^{13}C NMR spectrum (100 MHz) of compound **TTRO** in $CDCl_3$ at 298 K.

HR-MS spectra

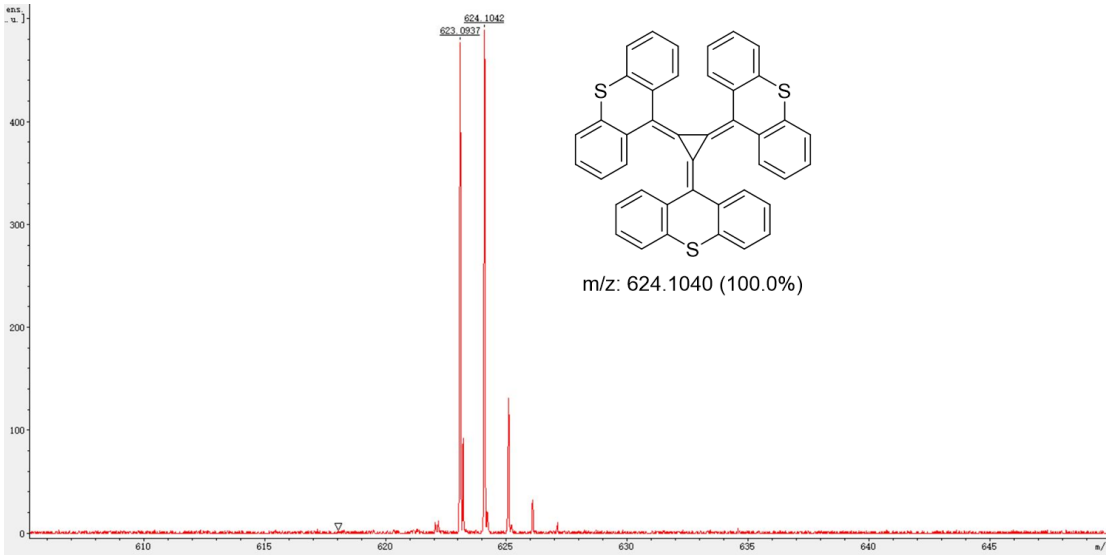

Figure S5. HR-MS of compound **TTR**.

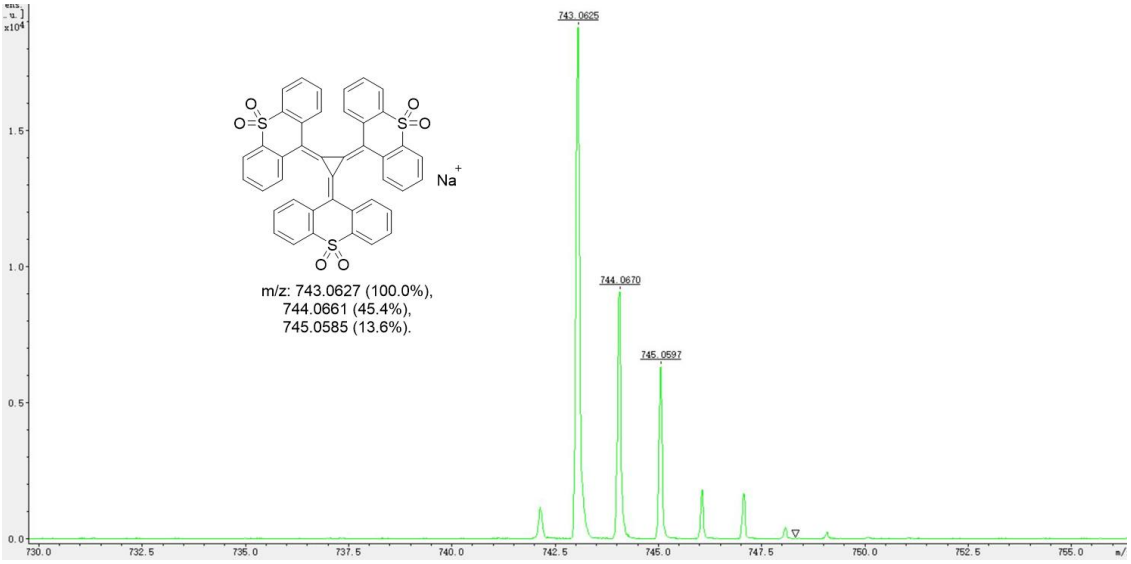

Figure S6. HR-MS of compound **TTRO**.

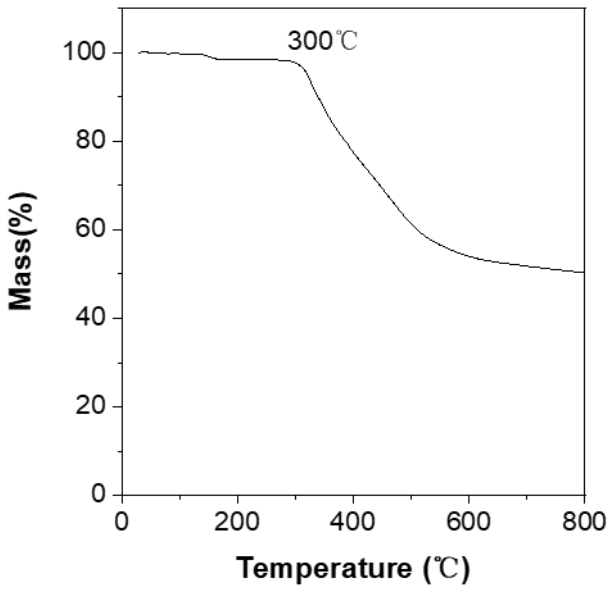

Figure S7. Thermogravimetric analysis (TGA) of **Hex@TTRO** polycrystalline solids

Note: *The preparation method for polycrystalline samples **TTRO** used in TGA and nitrogen adsorption tests differs from that of single crystal cultivation. Specifically, a saturated chloroform solution of **TTRO** is slowly added to n-hexane, resulting in the formation of polycrystalline samples of **TTRO*** immediately. *Powder XRD testing further confirmed the consistency of its stacking structure with the single crystal samples (**Figure S13**).*

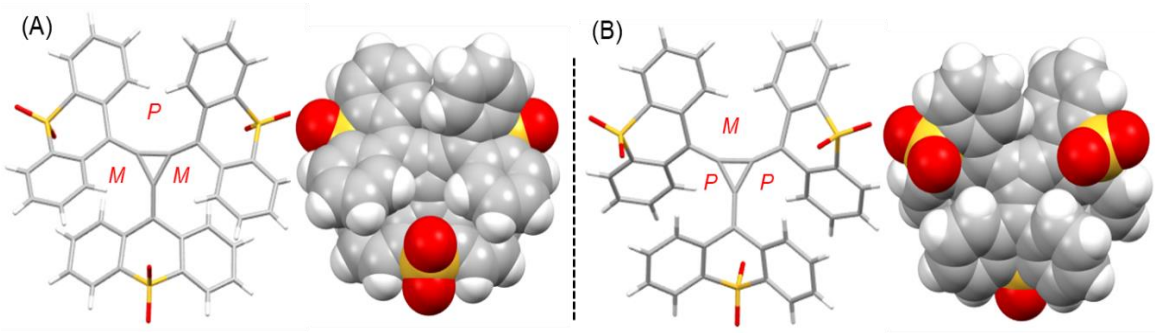

Figure S8. Chiral isomers present in the **Hex@TTRO** single crystal and corresponding spacefill mode.

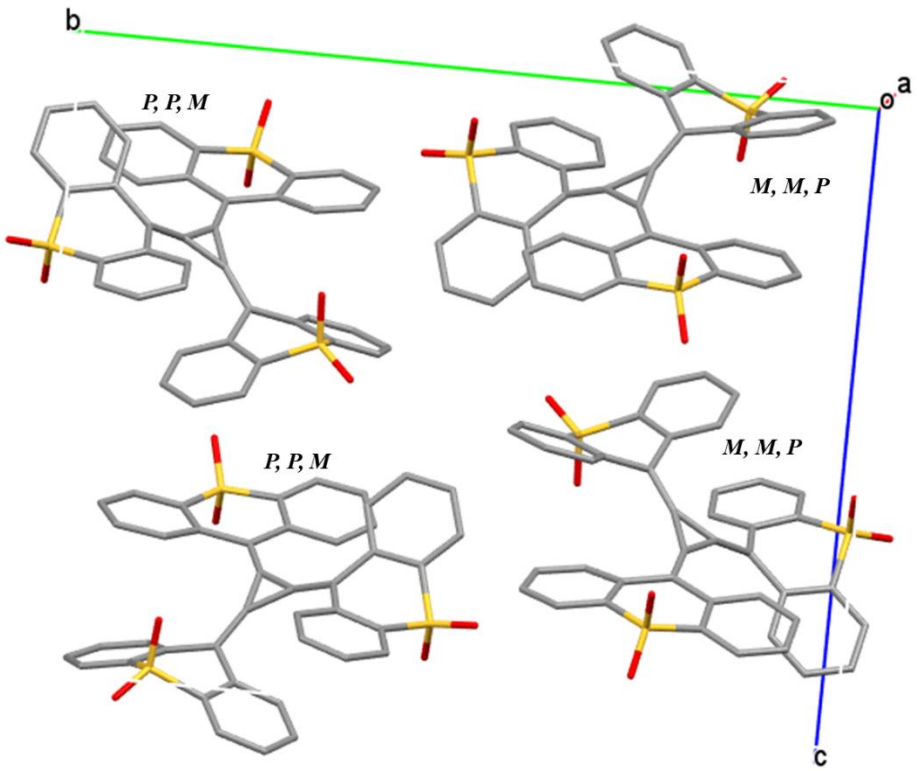

Figure S9. Unit cell of **Non@TTRO** single crystal containing two pairs of *P*/*M* isomers.

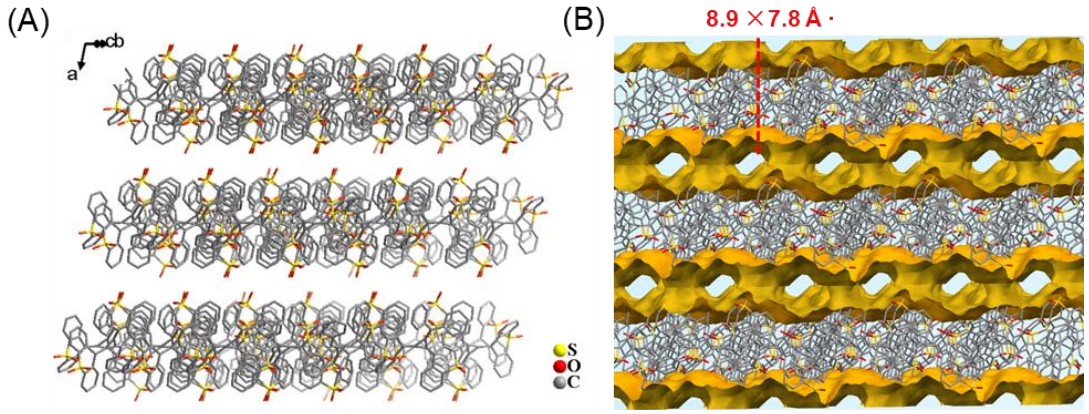

Figure S10. Crystal packing (A) and void space (B) of **Hex@TTRO**. This pore structure is in the same horizontal direction as Figure 2E-2F but viewed from a different angle.

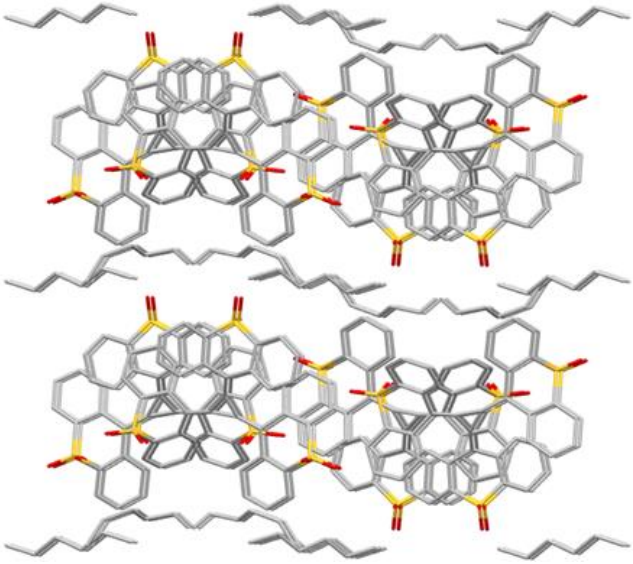

Figure S11. TTRO and Hexane packing mode in **Hex@TTRO** crystal.

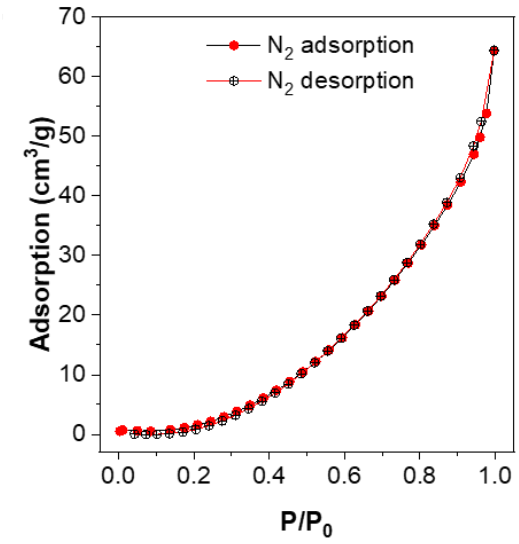

Figure S12. N_2 gas adsorption and desorption isotherm of **Hex@TTRO** polycrystalline solids.

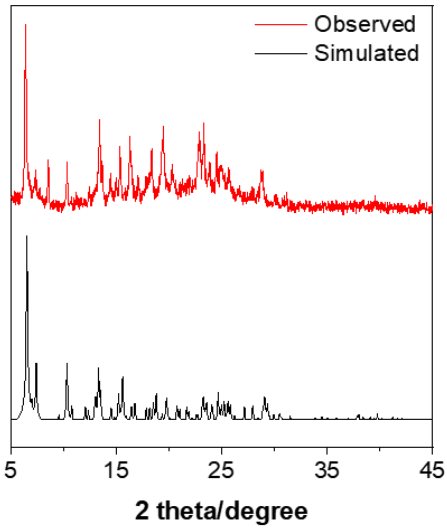

Figure S13. Simulated and experimental PXRD spectra of **TTRO** polycrystalline samples obtained from $CHCl_3$/Hexane chemical environment.

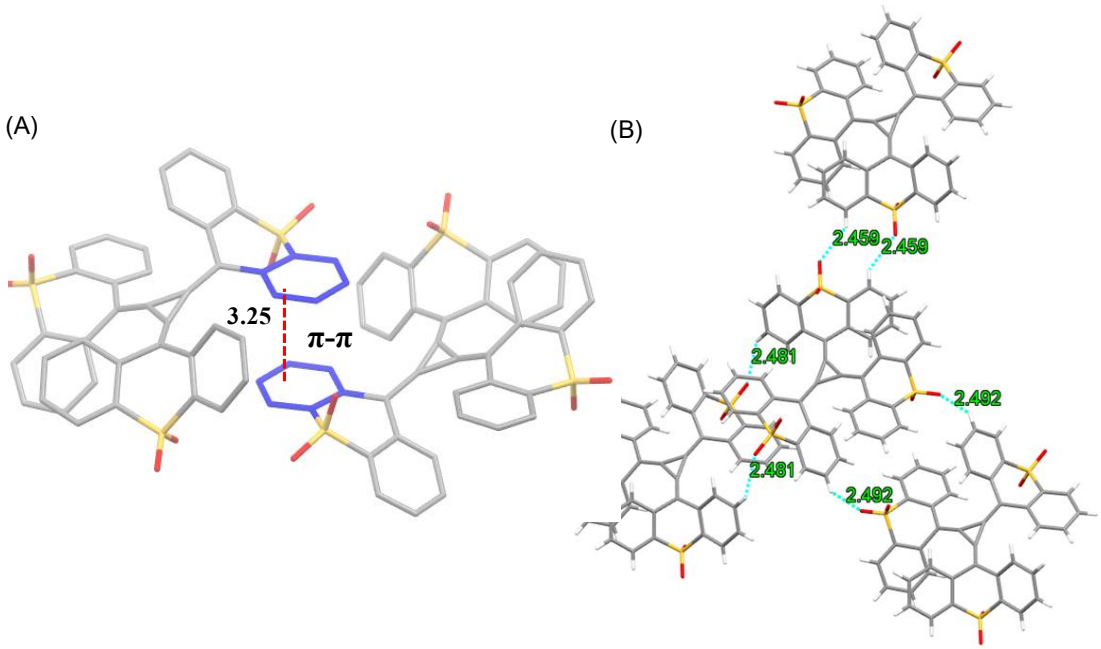

Figure S14. Intermolecular π-π (A) and C-H···O (B) interactions in **DMF/MeOH@TTRO** single crystal.

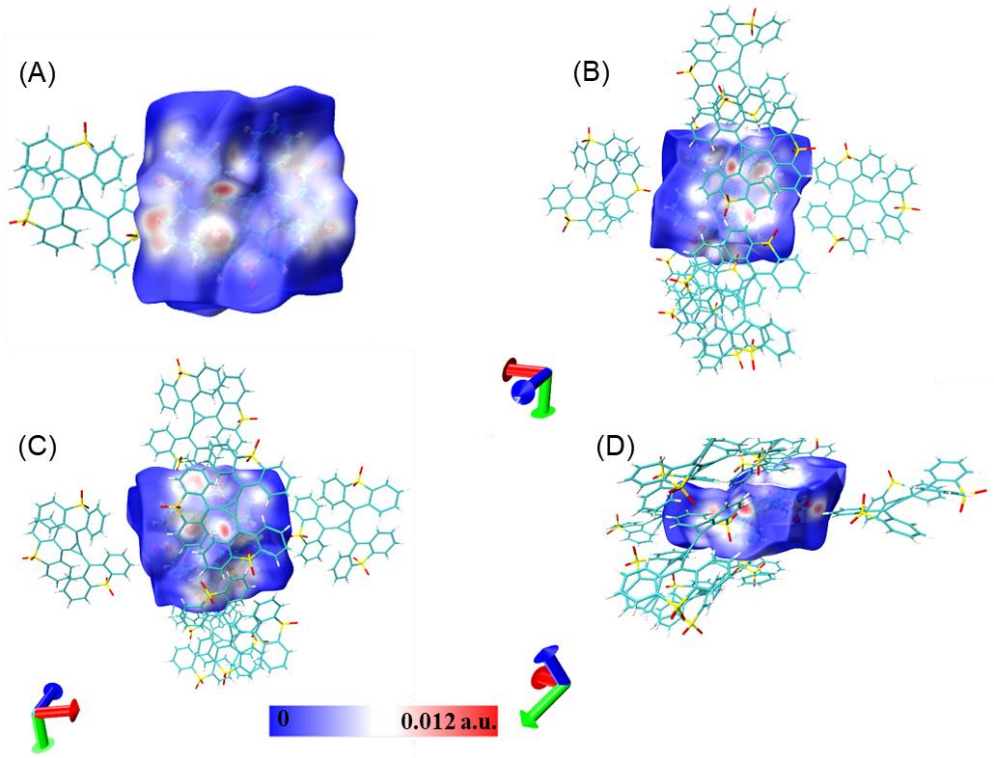

Figure S15. Hirshfeld surface analysis of **Hex@TTRO** crystal viewed from different direction.

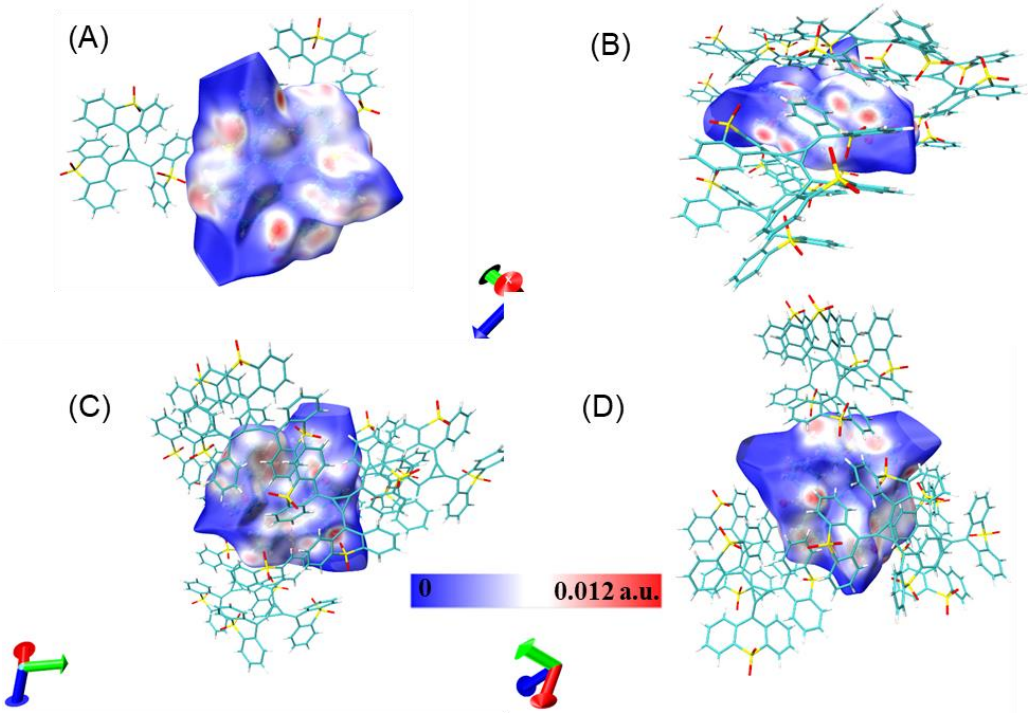

Figure S16. Hirshfeld surface analysis of **DMF/MeOH@TTRO** crystal viewed from different direction.

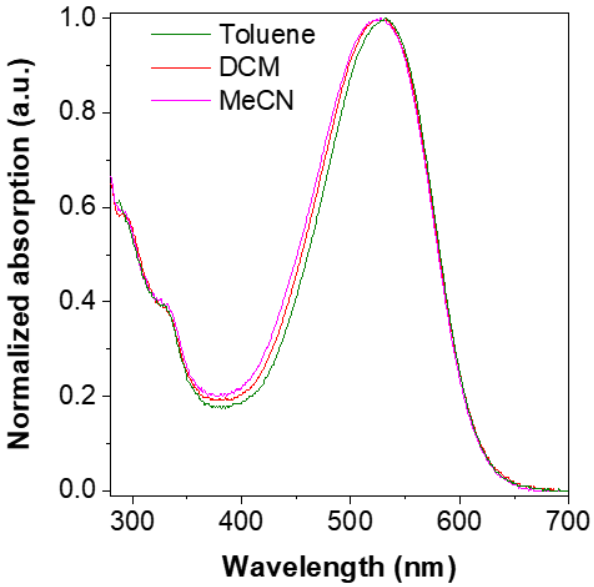

Figure S17. UV-vis absorption spectra of **TTRO** in different solvents.

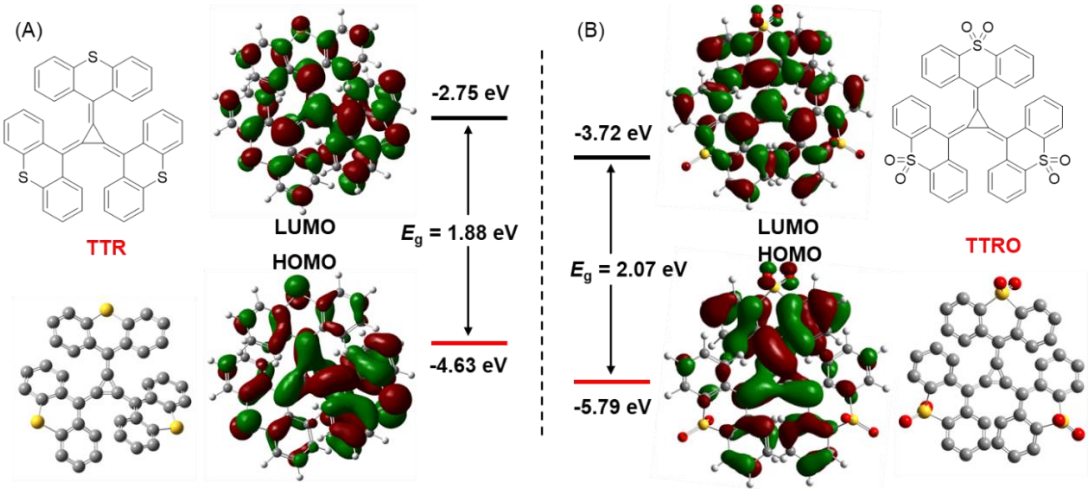

Figure S18. Molecular structure and molecular orbital amplitude plots of the HOMO (bottom) and LUMO (top) energy levels of **TTR** (A) and **TTRO** (B) calculated at the B3LYP/6-31G(d,p) level on basis of optimized structures.

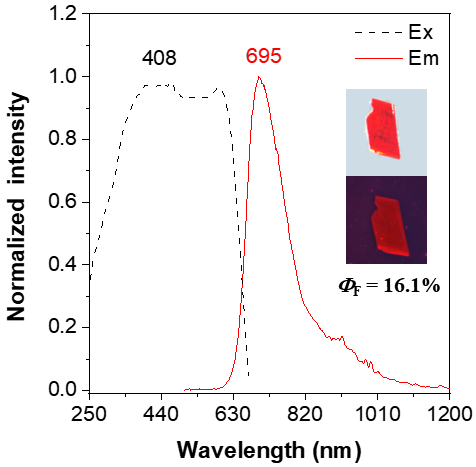

Figure S19. Normalized exciton and emission PL spectra of **Hex@TTRO** crystal sample.

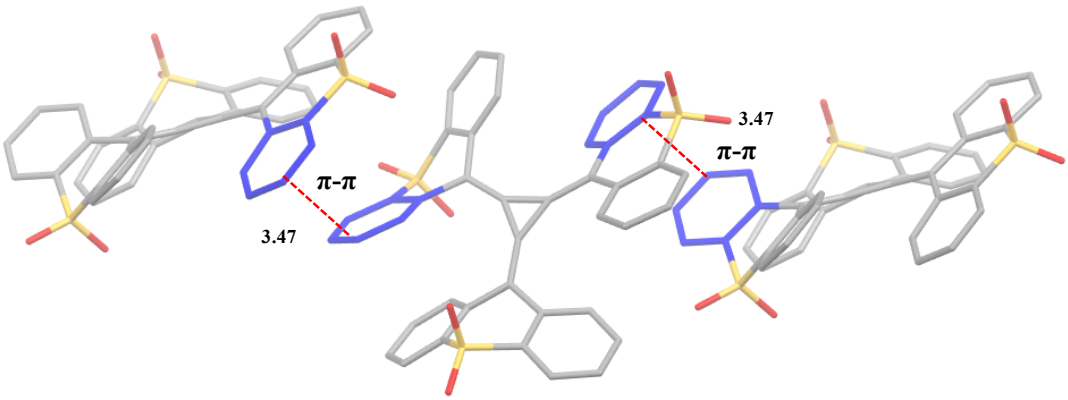

Figure S20. Intermolecular π-π interactions in **Non@TTRO** single crystal.

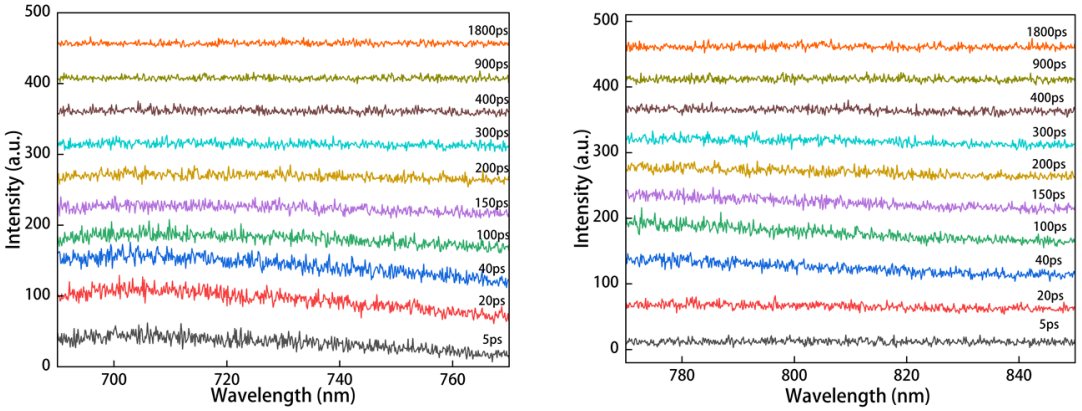

Figure S21. Ultrafast time-resolved PL spectra of **TTRO** amorphous powder collecting different emission wavelength range.

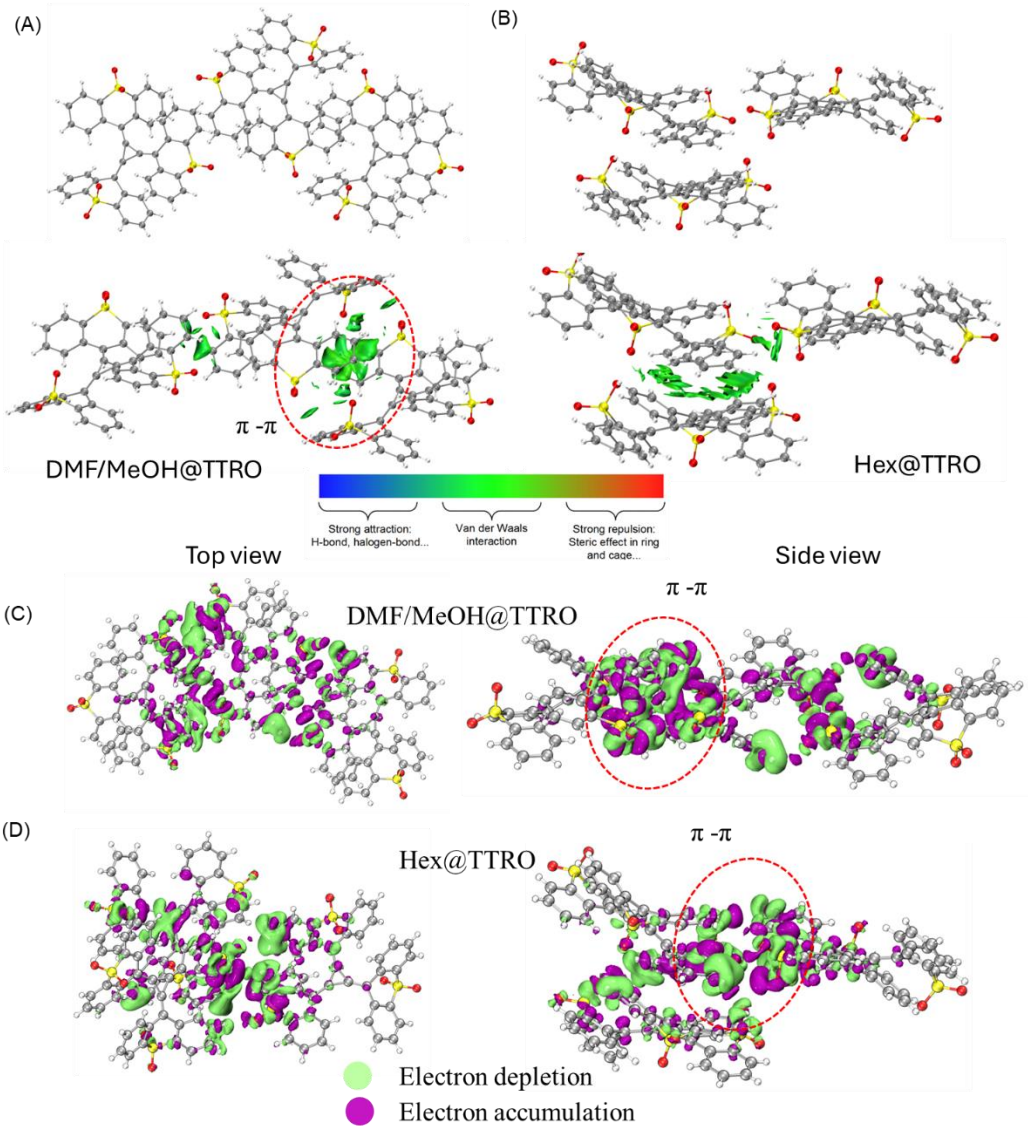

Figure S22. (A), (B) Trimer packing mode obtained from single crystal structure and study of weak intermolecular interactions via the Independent Gradient Model based on Hirshfeld partition (IGMH) for **DMF/MeOH@TTRO** (A), **Hex@TTRO** (B). Calculated Electron density differences maps between single molecule structure and trimer structure, **DMF/MeOH@TTRO** (C), **Hex@TTRO** (D).

Crystallographic data

Table S1 Crystal data and structure refinement of **Non@TTRO** (CCDC: 2476304).

Empirical formula	$C_4H_{2.29}O_{0.57}S_{0.29}$
Formula weight	68.65
Temperature/K	273(2)
Crystal system	monoclinic
Space group	$P2_1/n$

a/Å	7.868(4)
b/Å	22.623(15)
c/Å	18.246(13)
α /°	90
β /°	94.783(14)
γ /°	90
Volume/Å3	3236(3)
Z	42
ρ calcg/cm3	1.479
μ /mm-1	0.283
F(000)	1488.0
Crystal size/mm3	0.22 × 0.19 × 0.18
Radiation	MoKα (λ = 0.71073)
2Θ range for data collection/°	4.48 to 56.62
Index ranges	-9⩽h⩽10, -30⩽k⩽30, -24⩽l ⩽23
Reflections collected	42661
Independent reflections	8057 [Rint = 0.0406, Rsigma = 0.0322]
Data/restraints/parameters	8057/0/536
Goodness-of-fit on F2	1.079
Final R indexes [I>=2σ (I)]	R1 = 0.0439, wR2 = 0.1082
Final R indexes [all data]	R1 = 0.0574, wR2 = 0.1186
Largest diff. peak/hole / e Å^{-3}	1.22/-0.58

Table S2 Crystal data and structure refinement of **Hex@TTRO** (CCDC: 2476305).

Empirical formula	$C_{42}H_{24}O_6S_3$	
Formula weight	720.79	
Temperature	213 K	
Wavelength	0.71073 Å	
Crystal system	Monoclinic	
Space group	$P12_1/c_1$	
Unit cell dimensions	a = 14.4113(4) Å	α/°= 90°.
	b = 25.3415(8) Å	β/°= 109.4130(10)°.
	c = 12.3572(4) Å	γ/° = 90°.
Volume	4256.3(2) Å^3	
Z	4	
Density (calculated)	1.125 Mg/m^3	
Absorption coefficient	0.215 mm^{-1}	

F(000)	1488
Crystal size	0.2 x 0.15 x 0.13 mm^3
Theta range for data collection	2.197 to 25.998°.
Index ranges	-17<=h<=17, -31<=k<=31, -15<=l<=15
Reflections collected	43143
Independent reflections	8341 [R(int) = 0.0353]
Completeness to theta = 25.242°	99.6 %
Absorption correction	Semi-empirical from equivalents
Max. and min. transmission	0.7456 and 0.6531
Refinement method	Full-matrix least-squares on F^2
Data / restraints / parameters	8341 / 0 / 460
Goodness-of-fit on F^2	1.169
Final R indices [I>2sigma(I)]	R1 = 0.0446, wR2 = 0.1499
R indices (all data)	R1 = 0.0554, wR2 = 0.1600
Extinction coefficient	n/a
Largest diff. peak and hole e.$Å^{-3}$	0.230 and -0.315

Table S3 Crystal data and structure refinement **THF@TTRO** (CCDC: 2476306).

Empirical formula	$C_{44}H_{28}O_7S_3$	
Formula weight	764.84	
Temperature	296(2) K	
Wavelength	0.71073 Å	
Crystal system	Monoclinic	
Space group	$P2_1/c$	
Unit cell dimensions	a = 14.864(2) Å	a= 90°.
	b = 25.267(4) Å	b= 109.556(4)°.
	c = 12.5224(18) Å	g = 90°.
Volume	4431.8(11) $Å^3$	
Z	4	
Density (calculated)	1.146 Mg/m^3	
Absorption coefficient	0.212 mm^{-1}	
F(000)	1584	
Crystal size	0.200 x 0.200 x 0.200 mm^3	
Theta range for data collection	2.016 to 24.998°.	
Index ranges	-17<=h<=15, -30<=k<=28, -14<=l<=14	
Reflections collected	68148	

Independent reflections	7794 [R(int) = 0.1421]
Completeness to theta = 24.998°	99.9 %
Absorption correction	Semi-empirical from equivalents
Refinement method	Full-matrix least-squares on F^2
Data / restraints / parameters	7794 / 47 / 505
Goodness-of-fit on F^2	0.994
Final R indices [I>2sigma(I)]	R1 = 0.0901, wR2 = 0.2436
R indices (all data)	R1 = 0.1870, wR2 = 0.2939
Extinction coefficient	n/a
Largest diff. peak and hole	0.698 and -0.448 e.$Å^{-3}$

Table S4 Crystal data and structure refinement of **DMF/MeOH@TTRO** (CCDC: 2476303).

Empirical formula	$C_{42}H_{24}O_6S_3$
Formula weight	720.79
Temperature/K	100.01(10)
Crystal system	triclinic
Space group	P-1
a/Å	7.18920(10)
b/Å	16.6927(4)
c/Å	17.5904(4)
α/°	66.493(2)
β/°	89.947(2)
γ/°	89.447(2)
Volume/$Å^3$	1935.69(7)
Z	2
ρcalcg/cm^3	1.237
μ/mm^{-1}	2.121
F(000)	744.0
Crystal size/mm^3	0.3 × 0.2 × 0.1
Radiation	Cu Kα (λ = 1.54184)
2Θ range for data collection/°	5.478 to 133.184
Index ranges	$-8 \le h \le 8$, $-19 \le k \le 19$, $-20 \le l \le 20$
Reflections collected	26396
Independent reflections	6832 [Rint = 0.0343, Rsigma = 0.0305]

Data/restraints/parameters	6832/153/460
Goodness-of-fit on F^2	1.049
Final R indexes [I>=2σ (I)]	R1= 0.0419, wR2= 0.1002
Final R indexes [all data]	R1= 0.0464, wR2= 0.1018
Largest diff. peak/hole / e $Å^{-3}$	0.51/-0.55

Table S5. Selected Dihedral angle in four single crystal structures of **TTRO**.

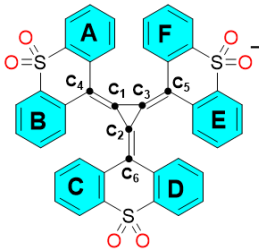

Dihedral angle	A,B	C,D	E,F
Hex@TTRO	26.2 °	43.2 °	51.3 °
THF@TTRO	25.4 °	44.0 °	50.9 °
DMF/MeOH@TTRO	35.9°	44.9°	49.2°
Non@TTRO	13.9°	44.4 °	38.4°

Table S6. Selected bond length in four single crystal structures of **TTRO**.

Selected bond length	Hex@TTRO (Å)	THF@TTRO (Å)	DMF/MeOH@TTRO (Å)	Non@TTRO (Å)
C1-C3	1.445	1.450	1.442	1.434
C1-C2	1.432	1.427	1.432	1.429
C2-C3	1.438	1.438	1.438	1.435
C1-C4	1.363	1.361	1.357	1.372
C3-C5	1.346	1.339	1.341	1.357
C2-C6	1.351	1.357	1.353	1.352

Table S7. Photophysical properties of different **TTRO** crystals.

Entry	λ_{ex} (nm)	λ_{em} (nm)	Φ_F[a] (%)	τ (ns)	χ^2	(k_r [10^8 s^{-1}], k_{nr} [10^8 s^{-1}])[b]
Hex@TTRO	408	695	16.1	2.7	1.13	(0.60, 3.11)
THF@TTRO	395	706	14.6	2.5	1.16	(0.56, 3.44)
Non@TTRO	365	685	-	-	-	-
DMF/MeOH@TTRO	380	698	24.1	1.4	1.06	(1.72, 5.42)

[a]measured by an integrating sphere; [b]k_r: radiative decay rate; k_{nr}: nonradiative decay rate.

Table S8. Photophysical properties for grounded and fumed **TTRO** samples.

Entry	λ_{em} (nm)	Φ_F[a] (%)	τ (ns)	τ_1 (ns)	τ_1 (ns)	τ_3 (ns)	χ^2
TTRO-G2	745	1.3	3.6	1.2(72.9%)	3.8(15.0%)	18.2(18.1%)	1.03
TTRO-G3	782	<0.1	-	-		-	-
TTRO-F3	735	3.1	2.6	0.8(77.1%)	3.4(13.3%)	15.5 (9.6%)	1.09

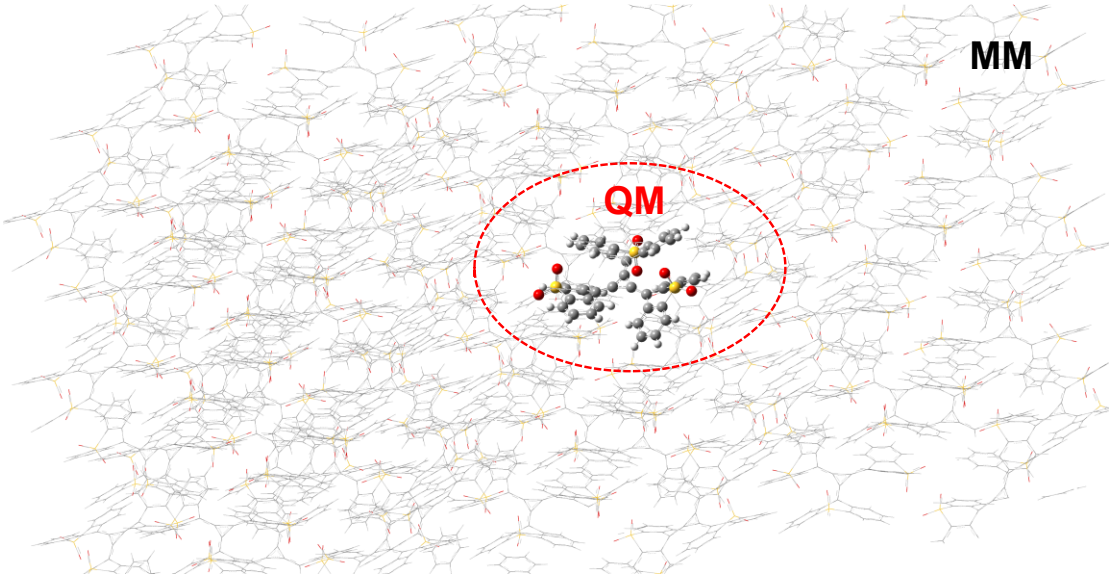

Figure S23. QM/MM model of **TTRO** for **Hex@TTRO** as an example. 108 molecules are included and the central one is treated as QM part and the surrounding one acts as the MM parts. In geometry optimization, the QM part is active and the MM part is frozen.

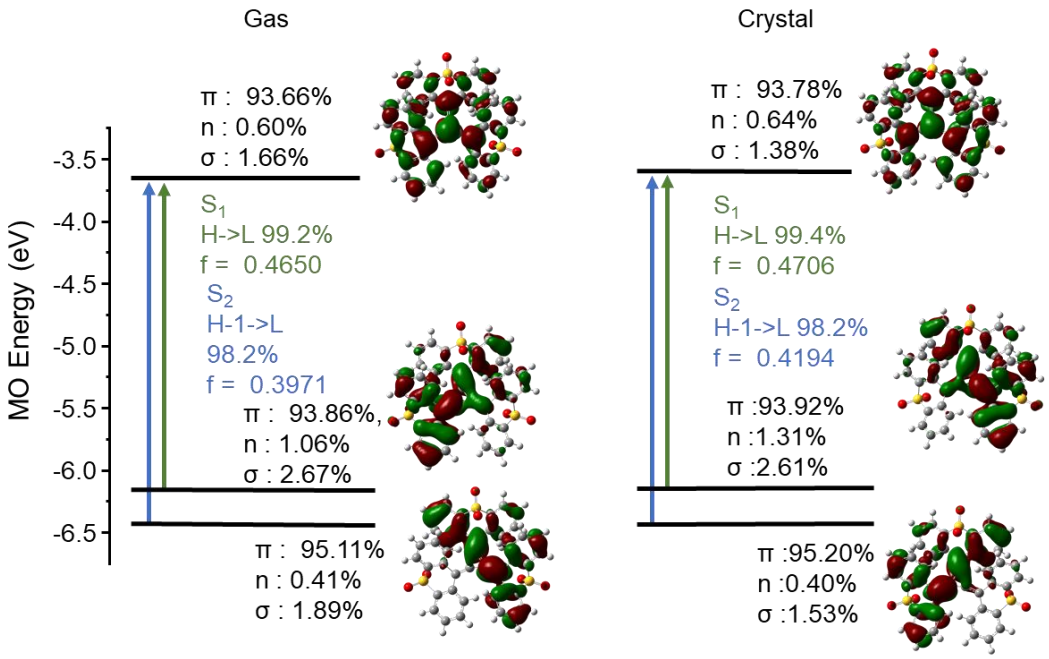

Figure S24 Involved molecular frontier orbital and their energy levels, transition property of the S_1 state and the oscillator strengths at the S_0-geometry in the gas and crystalline phases.

Table S9. Calculated vertical transition energy (E) and oscillator strength (*f*) and transition orbitals (TOs) of **TTRO** at the S_0-geometry in both the gas and solid phases.

S_0 geometry	**S_1**			**S_2**		
	f	*E*(eV)	Transition orbitals	*f*	*E*(eV)	Transition orbitals
Gas	0.4650	2.3508/ 527.41 nm	H -> L 99.2%	0.3971	2.5551/ 485.24 nm	H-1 -> L 98.2%
Crystal	0.4706	2.3402/ 529.80 nm	H->L 99.4%	0.4194	2.5541/ 485.43 nm	H-1->L 98.2%

Table S10. Calculated vertical transition energy (E) and oscillator strength (*f*) and transition orbitals (TOs) of **TTRO** at the S_1-geometry in both the gas and solid phases.

S_1 geometry	S_1			S_2		
	f	*E*(eV)	Transition orbitals	*f*	*E*(eV)	Transition orbitals
Gas	0.1577	1.2062/1027.89 nm	H -> L 107.4%	0.3495	1.9881/623.63 nm	H-1 -> L 99.9%
Crystal	0.3864	1.8368/675.00 nm	H -> L 101.6%	0.3850	2.1837/567.77 nm	H-1 -> L 98.9%

References

[S1] Spek, A., Single-crystal structure validation with the program PLATON. *J. Appl. Cryst.* **2003,** *36*, 7-13.

[S2] Gaussian 16, Revision A.03, M. J. Frisch, G. W. Trucks, H. B. Schlegel, G. E. Scuseria, M. A. Robb, J. R. Cheeseman, G. Scalmani, V. Barone, G. A. Petersson, H. Nakatsuji, X. Li, M. Caricato, A. V. Marenich, J. Bloino, B. G. Janesko, R. Gomperts, B. Mennucci, H. P. Hratchian, J. V. Ortiz, A. F. Izmaylov, J. L. Sonnenberg, D. Williams-Young, F. Ding, F. Lipparini, F. Egidi, J. Goings, B. Peng, A. Petrone, T. Henderson, D. Ranasinghe, V. G. Zakrzewski, J. Gao, N. Rega, G. Zheng, W. Liang, M. Hada, M. Ehara, K. Toyota, R. Fukuda, J. Hasegawa, M. Ishida, T. Nakajima, Y. Honda, O. Kitao, H. Nakai, T. Vreven, K. Throssell, J. A. Montgomery, Jr., J. E. Peralta, F. Ogliaro, M. J. Bearpark, J. J. Heyd, E. N. Brothers, K. N. Kudin, V. N. Staroverov, T. A. Keith, R. Kobayashi, J. Normand, K. Raghavachari, A. P. Rendell, J. C. Burant, S. S. Iyengar, J. Tomasi, M. Cossi, J. M. Millam, M. Klene, C. Adamo, R. Cammi, J. W. Ochterski, R. L. Martin, K. Morokuma, O. Farkas, J. B. Foresman, and D. J. Fox, Gaussian, Inc., Wallingford CT, (**2016**).

[S3] Lu, T., A comprehensive electron wavefunction analysis toolbox for chemists, Multiwfn. *J. Chem. Phys.,* 161, 082503 (**2024**) DOI: 10.1063/5.0216272.

[S4] Lu, T.; Chen, F., Multiwfn: a multifunctional wavefunction analyzer. *J. Comput. Chem.* **2012**, *33*, 580-92.

[S5] Grimme S, Ehrlich S, Goerigk L. Effect of the damping function in dispersion corrected density functional theory[J]. *J. Comput. Chem.*, **2011**, 32: 1456-1465.

[S6] Grimme S, Antony J, Ehrlich S, et al. A consistent and accurate ab initio parametrization of density functional dispersion correction (DFT-D) for the 94 elements H-Pu[J]. *J. Chem. Phys.*, **2010**, 132, 154104.

[S7] Weigend F, Ahlrichs R. Balanced basis sets of split valence, triple zeta valence and quadruple zeta valence quality for H to Rn: Design and assessment of accuracy[J]. *Phys. Chem. Chem. Phys.*, **2005**, 7: 3297-3305.

[S8] Weigend F. Accurate Coulomb-fitting basis sets for H to Rn[J]. *Phys. Chem. Chem. Phys.*, **2006**, 8: 1057-1065.

[S9] Lu T, Chen Q. Independent gradient model based on Hirshfeld partition: A new method for visual study of interactions in chemical systems[J]. *J. Comput. Chem.*, **2022**, 43: 539-555.

[S10] Humphrey, W.; Dalke, A.; Schulten, K., VMD: Visual molecular dynamics. *J. Mol. Graphics* **1996**, 14, 33-38.

[S11] Sarma, D.; Majumdar, B.; Sarma, T. K., Visible-light induced enhancement in the multi-catalytic activity of sulfated carbon dots for aerobic carbon–carbon bond formation. *Green Chem.* **2019,** *21*, 6717-6726.